Available online at www.sciencedirect.com
ScienceDirect
Journal of Catalysis 246 (2007) 91–99
JOURNAL OF CATALYSIS
www.elsevier.com/locate/jcat

Effects of manganese oxide promoter on the CO and H_2 adsorption properties of titania-supported cobalt Fischer–Tropsch catalysts

Fernando Morales, Emiel de Smit, Frank M.F. de Groot, Tom Visser, Bert M. Weckhuysen *

Inorganic Chemistry and Catalysis, Department of Chemistry, Utrecht University, Sorbonnelaan 16, 3584 CA Utrecht, The Netherlands

Received 6 October 2006; revised 3 November 2006; accepted 10 November 2006

Available online 22 December 2006

Abstract

The adsorption properties of manganese-promoted Co/TiO_2 Fischer–Tropsch (FT) catalysts were investigated by diffuse reflectance infrared spectroscopy (DRIFTS) using CO and H_2 as probe molecules. Manganese was found to be closely associated to the FT active Co^0 sites at the surface of the catalysts. With increased MnO loading, CO preferentially binded linearly to surface metal sites. Manganese also decreased the extent of Co–TiO_2 interactions, increasing the Co^0 dispersion, resulting in higher H_2 chemisorption uptake. Furthermore, with increasing MnO loading, FT catalytic tests at 1 bar and 220 °C revealed an increase in C_{5+} selectivity and olefinic products. These findings suggest that MnO species induce both structural and electronic promotion effects, resulting in higher metal dispersions and lower hydrogenation activity of the catalyst, ultimately enhancing the overall FT catalytic performance. The findings also suggest that MnO catalyzes the water–gas shift reaction, thereby changing the syngas feed composition and affecting overall catalyst performance.

Keywords: Fischer–Tropsch synthesis; Cobalt; Manganese; Promotion; DRIFTS

1. Introduction

Fischer–Tropsch (FT) technology, in which high molecular weight hydrocarbons are synthesized by catalytic hydrogenation of CO using Co-based catalysts, is to play a major role in the expected shift from crude oil to natural gas (GTL) and biomass (BTL) as feedstock for chemical industries [1–3]. An effective way to improve FT catalytic performance is to add small amounts of promoters to the catalyst materials [4]. Promoters have been shown to strongly affect the physicochemical and catalytic properties of the cobalt active sites and thus can be used to tune the reaction selectivity toward the desired product range distributions [4–7].

Recently, we have reported the benefits of using manganese as a promoter for Co/TiO_2 catalysts [5,7]. Adding small amounts of manganese was shown to improve the selectivity and in some cases the activity in the FT reaction. Advanced characterization techniques (e.g., in situ XAS, STEM-EELS, and XPS) have provided new insights into the active site composition and the state and location of the manganese promoter [5–8]. For instance, using manganese in Co/TiO_2 catalysts was found to decrease the amount of Co^0 surface atoms after reduction treatments [8], which has a clear impact on FT selectivity, such as suppression of CH_4 production. Furthermore, it has been shown that manganese can react with cobalt to form $Co_{3-x}Mn_xO_4$ mixed-oxide compounds, leading to decreased cobalt reducibility in the catalysts [6]. We also observed that reduction in H_2 results in redispersion of the cobalt phase and the formation of MnO species closely associated with Co^0 particles when catalysts were prepared using the homogeneous deposition precipitation (HDP) method [7]. Although the structural promotion effects of manganese have been widely reported, relatively few studies have focused on the electronic promoting effects of manganese on FT catalysts [9–12]. Therefore, at present the exact effect of manganese on the cobalt active sites and its role during the FT reaction remain somewhat unclear.

Infrared spectroscopy is a powerful technique for investigating the surface properties of catalysts, particularly their active sites, especially when used in combination with CO and CO/H_2 as probe molecules [13–18]. Manganese promotion in

* Corresponding author.
E-mail address: b.m.weckhuysen@chem.uu.nl (B.M. Weckhuysen).

0021-9517/$ – see front matter
doi:10.1016/j.jcat.2006.11.014

$RuMn/Al_2O_3$ [9], $CoMn/Al_2O_3$ [12], and unsupported Mn–Co [10] catalysts were previously studied by this technique. For the Co/TiO_2 system, conventional transmittance infrared spectroscopy is hardly possible due to a considerable drop in transmission after reduction treatments [19]. However, as has been demonstrated for Fe/Al_2O_3, Co/Al_2O_3 [20], and Co/TiO_2 catalysts [21], diffuse reflectance infrared spectroscopy (DRIFTS) is a useful alternative for studying low transmitting materials.

CO probe molecules can accept electron density from metal surface sites, resulting in metal–carbonyl complexes. These complexes are characterized by IR absorption bands at 2100–1800 cm^{-1}. The shift from the vibrational energy of gas-phase CO (2143 cm^{-1}) can be explained in terms of simple molecular orbital (MO) theory. The 5σ orbital of the CO molecule forms a σ bond with an empty orbital of the metal, and for electron-rich surfaces, back-donation from the metal d-orbitals into the antibonding π^*-orbitals of the CO molecule occurs, weakening the C≡O bond. The result is a red shift of the CO stretching frequency compared with "free" CO gas and the appearance of bands caused by CO linearly and bridged bonded to the cobalt metal surface. The precise position of these bands can provide valuable information about the electron density of the metal sites [9,22,23]. Furthermore, the intensity ratio of the linear and bridged bonded bands can be used as a measure for the electronic state of the Co nanoparticles [24].

In this study, CO and CO/H_2 mixtures were used to probe the surface of Co/TiO_2 catalysts promoted with different amounts of MnO. The objective of this work was to characterize, in a systematic way, the surfaces of Co/TiO_2 catalysts altered with increasing amounts of manganese. By monitoring the position of the absorption bands of surface-bonded CO molecules, we have obtained information on the nature of the surface cobalt sites before and during the FT reaction. Additional characterization of the catalysts was done with XRD, TPR, TEM, and H_2-chemisorption to investigate other physicochemical properties of the catalysts. In addition, catalytic performance for FT was measured (1 bar, 220 °C, $H_2/CO = 2$) to evaluate the changes in activity and selectivity after addition of MnO.

2. Experimental

2.1. Catalyst preparation

Cobalt (∼8 wt%) was deposited onto a TiO_2 support (Degussa P25, surface area 45 m^2/g, pore volume 0.27 cm^3/g) according to the HDP method [25], using cobalt nitrate (Merck) precursor solutions and urea (Acros) as the precipitation agent. The TiO_2 powder was suspended in an aqueous solution containing cobalt nitrate, and the pH was slowly increased by urea decomposition at 90 °C under continuous stirring for 18 h. After filtering the solution and drying the solid at 120 °C overnight, the precursor material was loaded with various amounts of manganese (1.21, 2.15, 2.89, and 2.95 wt%) by the incipient wetness impregnation (IWI) method. Finally, the samples were calcined in air flow at 400 °C for 4 h (at a heating ramp of 10 °C/min) to obtain the oxidized catalyst precursors coded as HCo_xMn_y, where x and y refer to the relative amounts of Co and Mn, respectively. An overview of the catalysts and their respective metal loadings is presented in Table 1.

2.2. Catalyst characterization

Cobalt and manganese loadings in the calcined catalysts were determined by X-ray fluorescence (XRF) using a Spectro X-lab 2000 instrument. The same materials were analyzed by X-ray diffraction (XRD) using an Enraf-Nonius CPS 120 XRD apparatus equipped with a curved position-sensitive INEL detector and a CoK_{α_1} radiation source ($\lambda = 1.78897$ Å). The line broadening of the Co_3O_4 diffraction peaks localized at 70° and 77° 2θ values was used to estimate the crystallite sizes, according to Scherrer's equation.

Temperature-programmed reduction (TPR) experiments were performed with Micromeritics Autochem-II instrument equipped with a thermal conductivity detector (TCD). The samples were initially dried in an Ar flow at 120 °C for 20 min; once the TCD signal was stable, the gas stream was switched to 5% H_2/Ar, and the temperature was raised from 40 to 700 °C at a rate of 10 °C/min.

Reduced and passivated HCo, $HCo_{20}Mn_3$, and $HCo_{20}Mn_5$ samples were analyzed by transmission electron microscopy (TEM) in a Tecnai 20 FEG TEM microscope operating at 200 kV and equipped with an EDX analyzer. About 50 mg of each catalyst was pretreated in a tubular glass reactor (3 mm diameter). The samples were dried in a flow of air at 120 °C for 30 min and subsequently reduced in a 50% H_2/He flow at 350 °C for 2 h (at a heating ramp of 5 °C/min). Passivation was carried out at 150 °C in a flow of 20% CO_2/He for 30 min. After passivation, the samples were unloaded from the reactor, crushed, ultrasonically dispersed in ethanol, and dropped on a holey carbon film on a copper grid for TEM analysis.

H_2 chemisorption measurements were carried out using a Micromeritics ASAP 2010C instrument. Before the measurements were started, the samples were dried in a He flow at 120 °C for 30 min, followed by reduction in a 50% H_2/He flow at 350 °C for 2 h (ramp = 5 °C/min). The H_2 adsorption isotherms were measured at 150 °C, the temperature recommended by Reuel and Bartholomew [26]. The percentage cobalt dispersion was calculated assuming complete reduction and a stoichiometry of one hydrogen atom adsorbed per cobalt surface atom [26].

DRIFTS experiments were carried out using a Perkin–Elmer FTIR 2000 series infrared spectrometer at a resolution of 4 cm^{-1}; 50 scans were accumulated for each spectrum. The spectrometer was equipped with a Harrick "Praying Mantis" DRIFTS accessory along with a reactor cell with CaF_2 windows. The powdered samples were loaded in the reactor cell and reduced in a H_2 flow at 350 °C for 2 h (at a heating rate of 5 °C/min). Subsequently, the samples were cooled to room temperature in a He flow. At this temperature, a background spectrum was recorded. Next, CO was fed to the cell for 30 min. DRIFT spectra were recorded after purging the cell with He. For the CO/H_2 adsorption experiments, the samples were activated using the same reduction procedure. After reduction, the temperature was decreased to 220 °C in flowing He. Back-

Table 1
Physicochemical properties of the Co-based FT catalyst materials under study together with the XRD, TEM, and H_2 chemisorption results

Sample code	Co[a] (wt%)	Mn[a] (wt%)	XRD peak maximum	Co_3O_4 size[b] (nm)	H_2 uptake (mmol/g)	Co (%) dispersion	TEM (nm)
HCo	7.77	0.0	77.36	24.7	0.010	1.23	2–7
$HCo_{20}Mn_2$	7.01	1.21	77.28	24.0	0.024	3.02	–
$HCo_{20}Mn_3$	6.98	2.15	77.18	19.2	0.037	4.63	2–10
$HCo_{20}Mn_4$	7.12	2.89	77.09	11.3	0.021	2.67	–
$HCo_{20}Mn_5$	6.54	2.95	77.20	14.0	0.017	2.20	2–6

[a] Determined by XRF, assuming the Co and Mn to be present in the form of Co^0 and MnO.
[b] Calculated from the average values obtained between the reflections located at 70° and 77° 2θ values.

ground spectra were collected before the gas feed was switched to CO/H_2 mixture (1/2 v/v). DRIFT spectra were continuously recorded during 2 h of reaction. Finally, the cell was purged with He once again, and additional spectra were measured.

2.3. Catalyst testing

Catalysts were tested at 1 bar and 220 °C using CO/H_2 (1/2 v/v) after reduction treatments in H_2 at 350 °C for 2 h. Typically, 50 mg of catalyst sample (particle size, 0.21–0.50 mm) was diluted in SiC (particle size, 0.22 mm) to prevent temperature gradients within the catalyst bed, and then loaded into a tubular glass fixed-bed reactor (diameter, 3 mm). The reactor was placed in a tubular quartz oven, and the temperature inside and near the bottom of the catalyst bed was monitored using 2 type-K thermocouples. Gas hourly space velocities of 3010 h^{-1} were used in all experiments, leading to CO conversions of ∼1%. Product analysis (C_1–C_{20}) was carried out on-line using a Varian CP-3800 gas chromatograph equipped with a flame ionization detector and fitted with a 50-m CP-Sil 5 CB column. All reactor lines were maintained at 130 °C to prevent the condensation of heavier hydrocarbon products. All reaction products were analyzed from the gas (vapor) phase.

3. Results and discussion

3.1. Manganese as structural promoter element

XRD patterns obtained for the Co/TiO_2 and $Co/Mn/TiO_2$ oxidized samples are displayed in Fig. 1. Distinct diffraction lines originating from TiO_2 (anatase and rutile phases) can be observed, as can other small lines centered at 36°, 52°, 70°, and 77° 2θ values, corresponding to a Co_3O_4 phase. The latter peaks are clearly wider than those originating from TiO_2, indicating smaller-sized Co_3O_4 crystallites. On the other hand, the Co_3O_4 reflections become weaker with increasing manganese loading. This effect is attributed to a loss of crystallinity as a result of the interaction between Co_3O_4 and manganese to form a $Co_{3-x}Mn_xO_4$-type solid solution [6,7,27]. The existence of Co–Mn-mixed species is also suggested by the position of the Co_3O_4 reflections, which all appear at slightly smaller 2θ values in the Mn-promoted catalysts. The latter phenomenon results from a decrease in the cell parameter on incorporation of Mn^{3+} into the Co_3O_4 lattice [28]. The Co_3O_4 particle sizes estimated from the diffraction peaks at 70° and 77° 2θ values vary

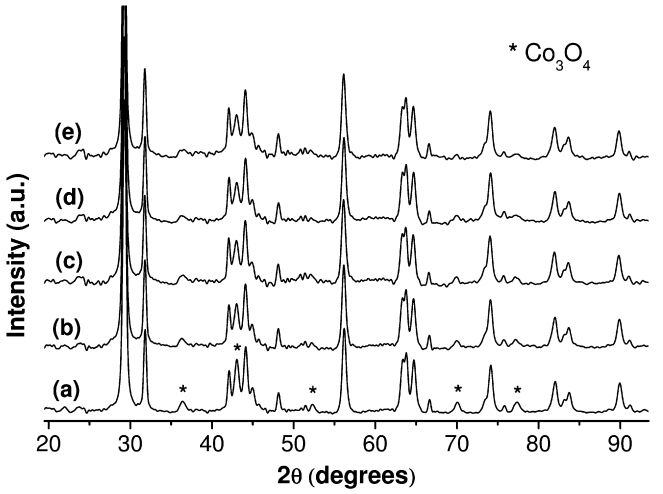

Fig. 1. XRD patterns of the HCo (a), $HCo_{20}Mn_2$ (b), $HCo_{20}Mn_3$ (c), $HCo_{20}Mn_4$ (d), and $HCo_{20}Mn_5$ (e) catalysts after the calcination treatment.

from 24 nm in HCo to around 11–14 nm in the Mn-promoted catalysts (Table 1). Note that because adding manganese affects the crystallinity of Co_3O_4 particles, the particle sizes calculated by Scherrer's equation are not completely accurate, because of the neglected contribution of crystallite strain to the diffraction line broadening. However, the large differences in the Co_3O_4 particle sizes indicate that manganese affects both the size and crystallinity of the Co_3O_4 particles as a result of a physicochemical interaction between these compounds during the calcination treatment.

The TPR reduction results for all samples presented in Fig. 2 show 3 distinct peaks centered around 275, 350, and 450 °C, corresponding to a 2-step reduction process from Co_3O_4 to CoO and Co^0 [7,8]. Because the catalysts were calcined before TPR analysis, organic or nitrate residues are not expected, and all TPR peaks can be unambiguously assigned to the reduction of cobalt species. Analysis of the peak areas indicates that the first peak originates from the reduction of Co_3O_4 to CoO, whereas the other two peaks stem from the subsequent reduction to Co^0. As revealed by the TPR profiles, manganese hampers the reduction of CoO to Co^0 in the Mn-promoted catalysts, as indicated by the higher relative intensity of the peak centered at 450 °C.

Due to the presence of mixed Co–Mn oxides, as already suggested by the XRD results, we considered a reliable quantification of the peak areas infeasible. The results are in good

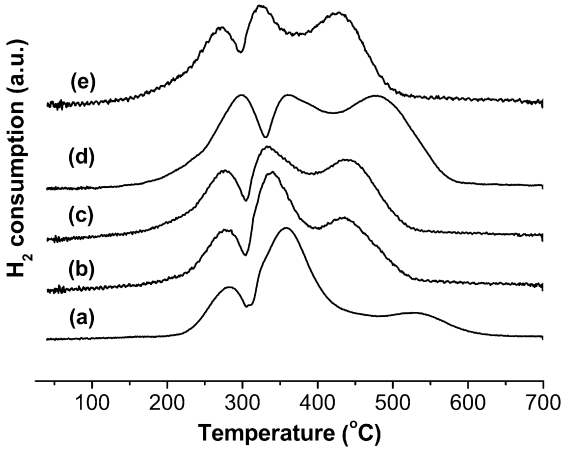

Fig. 2. TPR profiles of the calcined HCo (a), $HCo_{20}Mn_2$ (b), $HCo_{20}Mn_3$ (c), $HCo_{20}Mn_4$ (d), and $HCo_{20}Mn_5$ catalysts (e).

agreement with our previous studies, from which we concluded that adding manganese to Co/TiO_2 catalysts decreased cobalt reducibility and, consequently, segregation over the TiO_2 surface during the reduction process [7].

The size and morphology of the cobalt particles resulting after reduction and passivation of the HCo, $HCo_{20}Mn_3$, and $HCo_{20}Mn_5$ samples was studied by TEM. In Figs. 3–5, representative images of the three catalysts show supported cobalt (oxide) particles with spherical shapes and a broad size distribution. The TiO_2 particles can be seen enclosed in cobalt particles, which are more easily distinguished from the support material at the exterior surface. Cobalt particles generally vary in size from approximately 2 to 7 nm, with some larger agglomerates (∼8–15 nm) seen in HCo and $HCoMn_3$ catalysts (Figs. 3, 4). These agglomerates are composed of smaller cobalt particles. Note that the cobalt particles are more easily distinguished from the TiO_2 surface in the Mn-free sample. Adding manganese somewhat lowers the contrast between the support and the cobalt particles after reduction. Our previous studies [6] revealed strong manganese segregation over the TiO_2 surface on reduction treatments.

For all of the catalyst samples, the reduced (and passivated) cobalt particle sizes seen on TEM are somewhat smaller than would be expected from the cobalt oxide particles sizes found by XRD. Clearly, the large decrease in particle size on reduction cannot be explained simply by the loss of lattice oxygen from the cobalt oxide. Instead, it is suggested that the reduction treatment causes redispersion of the cobalt phase, most likely due to strong Co–TiO_2 interactions [29–31].

H_2 chemisorption measurements were carried out to determine the number of available surface Co^0 sites in the reduced catalysts. The H_2 uptakes and cobalt dispersions for the five samples are listed in Table 1. Significantly, the cobalt particle sizes calculated from the dispersions are much larger than those obtained from TEM analysis. For example, from H_2 chemisorption experiments, a dispersion of 1.23% was obtained for the HCo catalyst. Using the formula $d = 81.6W/X$, with d the particle size in nm, W the weight percentage of cobalt, and X the total H_2 uptake in micromoles per gram of catalyst [26], this dispersion would correspond to a particle size of 78 nm. This does not agree with the XRD Co_3O_4 particle size and TEM data. Calculating particle sizes from H_2 chemisorption data is justified only when cobalt is fully reduced and all surface sites are accessible. Thus, we attribute the difference in particle sizes obtained from TEM and H_2 chemisorption to incomplete cobalt reduction and/or masking of active surface sites, resulting in suppression of the amount of H_2 chemisorbed and subsequent miscalculation of dispersion and particle sizes.

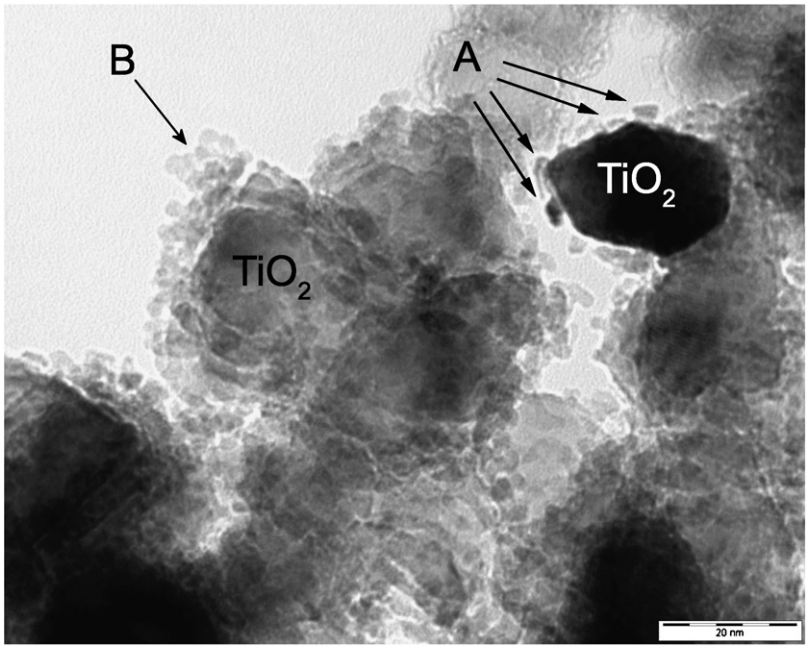

Fig. 3. TEM image of the reduced HCo catalysts, showing the presence of very small cobalt particles (A) (∼2–7 nm) covering the TiO_2 surface. In addition, some larger cobalt agglomerates (∼8–15 nm) can be also observed (B).

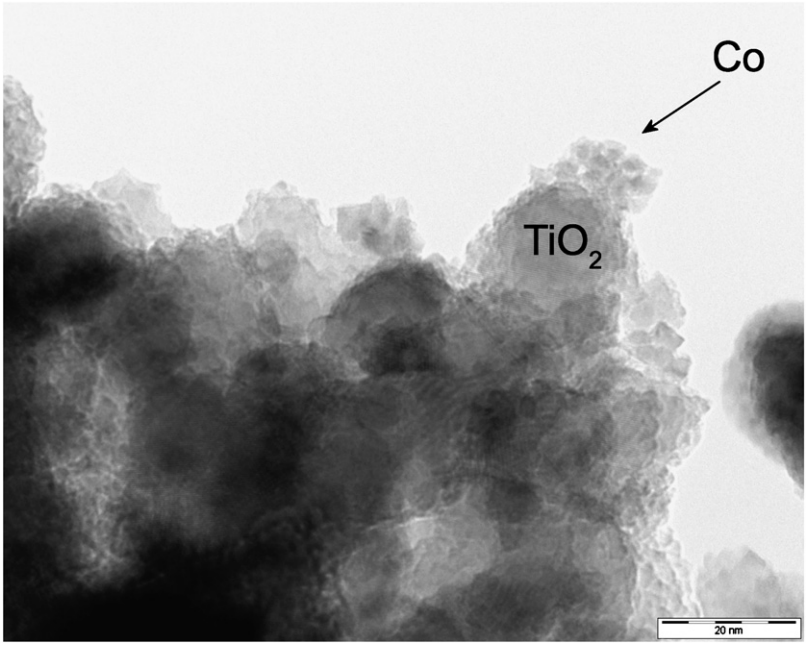

Fig. 4. TEM images of the reduced $HCo_{20}Mn_3$ catalysts, showing the presence of very small cobalt particles (∼2–10 nm) not so well distinguished from the TiO_2 surface. A large cobalt agglomerate is indicated by the arrow.

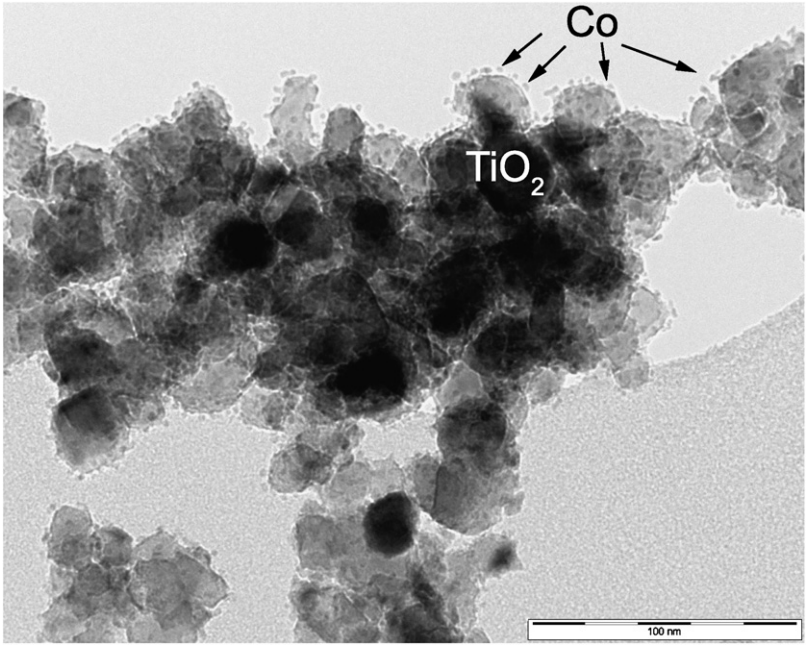

Fig. 5. TEM image of the reduced $HCo_{20}Mn_5$ catalyst, showing the presence of small (∼2–6 nm) cobalt particles at the TiO_2 surface as indicated by the arrows.

Comparing our results with reported data on cobalt supported on CNF catalysts [32–34] suggests that TiO_2 is responsible for the decreased cobalt reducibility. It is well known that strong metal–support interaction (SMSI) effects can occur when TiO_2 is used as a support material [29–31]. SMSI effects originate from a partial reduction of the TiO_2 surface during reduction treatment, leading to the formation and migration of TiO_x species over the catalyst surface. The formation and migration of TiO_x overlayers could indeed cause a masking of surface Co^0 sites and thereby decrease H_2 chemisorption uptake, leading to the calculation of very low dispersions and very large particle sizes.

H_2 uptake increases in the MnO-promoted catalysts with manganese loadings of 1.21 and 2.15 wt%, after which it decreases again with higher loadings. Because a fraction of the MnO spreads over the TiO_2 surface during reduction, it might prevent to some extent the SMSI effects of TiO_2 on Co^0 surface sites, thereby increasing H_2 uptake. At higher manganese loadings, however, MnO begins to cover cobalt surface sites as well, lowering H_2 uptake.

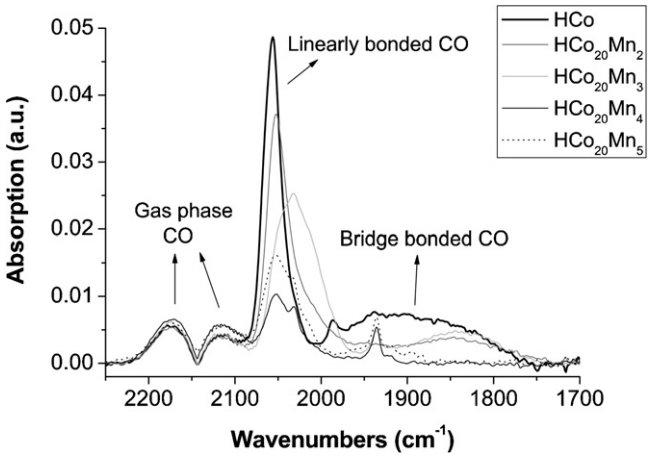

Fig. 6. DRIFTS spectra measured after CO adsorption at RT for the various Co/TiO_2 and $Co/Mn/TiO_2$ catalysts reduced at 350 °C.

3.2. Manganese as electronic promoter element

Fig. 6 shows the DRIFTS spectra obtained after CO adsorption on the different catalysts. Next to the rotational/vibrational transitions of the CO gas-phase molecules around 2173 and 2108 cm^{-1}, the region between 2060 and 1990 cm^{-1} reflects the stretching vibrations of CO linearly bonded to the surface cobalt metal sites [14,20,21,35]. Peak fitting of the band observed in this region revealed the presence of at least two different peaks, which points to different Co^0 surface sites. The peaks have a more or less fixed position around 2050 and 2030 cm^{-1}. For $HCo_{20}Mn_3$, even a third peak at 2010 cm^{-1} and hence a third type of Co^0 surface site is observed. The spectral region, roughly between 1900 and 1700 cm^{-1}, is commonly assigned to twofold, threefold, and possibly fourfold bridge-bonded CO to cobalt metal sites [12,21]. In most cases, the CO bridge-bonded peak exhibits a band maximum centered around 1850 cm^{-1}. An additional sharp absorption band at 1935 cm^{-1} is observed in the spectra of the catalysts with the highest manganese loadings ($HCo_{20}Mn_3$, $HCo_{20}Mn_4$, and $HCo_{20}Mn_5$). According to the literature, this peak most likely originates from CO interacting with manganese oxide species on the TiO_2 support [36].

As shown in Fig. 6, the spectral pattern significantly changes with increasing MnO content. These changes demonstrate that manganese affects the CO adsorption properties of the Co sites, pointing to a direct interaction with the Co particles. As was already demonstrated in a previous study [6] and described for the Co/SiO_2 [11] and $RuMn/Al_2O_3$ system [9], a fraction of the manganese remains located at the surface of the Co particles after reduction, thereby influencing the adsorption properties. MnO can interact both structurally and electronically with the cobalt active phase, and the observations in the DRIFTS spectra can be ascribed to both kinds of interactions.

In principle, three effects on the CO band pattern can be distinguished. The first effect is a decrease in total CO adsorption at higher MnO loadings. This indicates that fewer cobalt surface sites are available for binding CO, most likely due to masking by MnO species. This result has also been reported for manganese-promoted Ru/Al_2O_3 [9] and Co/Al_2O_3 [12] catalysts. Similar to the IR results, a drop in H_2 uptake and FT activity at the highest manganese loadings (2.89 and 2.95%) also pointed to a masking effect.

The second effect is the disappearance of bridge-bonded CO species on increasing MnO amounts. A possible explanation for this could be the increasing Lewis acidity of the Co^0 phase as result of an electronic effect of Mn^{2+} in MnO. According to the literature, a measure of the Lewis acidity of cations is the Kamlet–Taft parameter, which expresses a cation's ability to accept an electron pair. A high value corresponds to a strong Lewis acid character. Mn^{2+}, with a Kamlet–Taft value of 4.28 [15], is a strong Lewis acid and thus can withdraw electron density from the Co^0 phase. As a result, fewer bridge-bonded CO species are observed. Further research, involving the addition of promoters with varying Lewis acidity, is needed to support our findings. However, earlier CO adsorption infrared studies on promotion effects in zeolite-supported platinum metal particles have confirmed a correlation between the Lewis acidity of the promoter element and the relative amount of bridge-bonded CO species [17].

The third effect of the increasing MnO content is a change in the intensity ratio of the linearly bonded CO bands at 2030 and 2050 cm^{-1}. This effect cannot be readily explained as an electronic or a structural effect. From the σ-donation π^*-back donation model, we would expect some blue-shift of the C≡O stretching vibration on lowering the electron density of the cobalt metal phase, but hardly any frequency effect is observed. This effect is possibly related to the observation of increased H_2 uptake and catalytic activity in the sense that relatively more 2030-cm^{-1} cobalt adsorption sites become available as the SMSI interactions are reduced, and the dispersion of the catalyst is increased. Thus, it can be considered a structural effect of the MnO. Alternatively, MnO species might interact directly with the adsorbed CO molecules in the catalyst with higher manganese loadings, thereby weakening the C–O bond. In this case, it could be considered an electronic interaction between MnO and the cobalt phase. It should be stressed, however, that conclusive evidence for either case has not been found.

DRIFTS was also applied to study the catalysts under FT catalytic test conditions. The spectra shown in Figs. 7 and 8 correspond to species adsorbed at the catalyst surfaces after 2 h of exposure to H_2/CO mixtures at 220 °C. Although hydrocarbon species were observed at 3000–2800 cm^{-1}, we do not consider this region in detail due to the complex equilibrium of continually adsorbing and desorbing hydrocarbon chains. Two main spectral regions were evaluated: the CO absorption region (2250–1700 cm^{-1}), as discussed earlier, and the carbonate absorption region (1650–1300 cm^{-1}).

The CO stretching region at 2250–1700 cm^{-1} (Fig. 7) shows a broad peak centered at around 2020 cm^{-1} that can be assigned to CO linearly adsorbed to cobalt metal sites. The band maximum shifts from 2012 to 2031 cm^{-1} with increasing manganese loading. This blue-shift is in accordance with the earlier-described model in which the presence of Mn^{2+} at the surface of the Co^0 particles lowers its electronic density, which results in decreased back-donation into the antibonding π^* orbital of

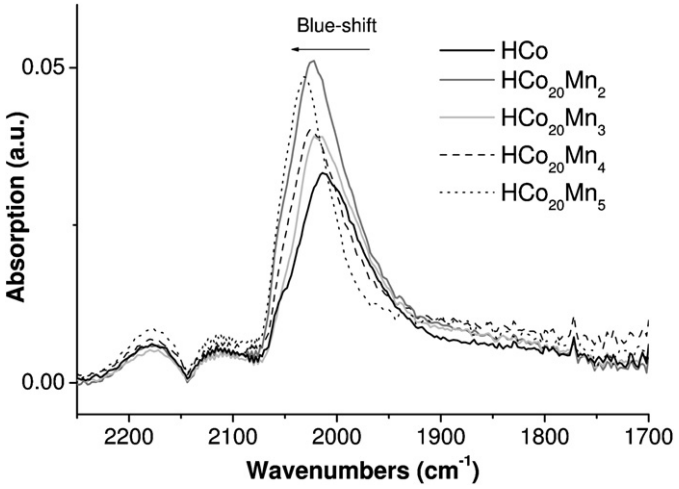

Fig. 7. DRIFTS spectra of the CO region for the different Co/TiO_2 and $Co/Mn/TiO_2$ catalysts after 2 h exposure to H_2/CO gas mixtures.

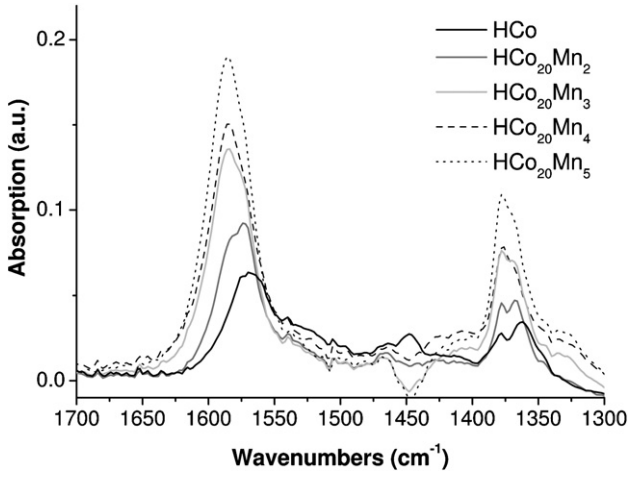

Fig. 8. DRIFTS spectra of the carbonate region for the different Co/TiO_2 and $Co/Mn/TiO_2$ catalysts after 2 h exposure to H_2/CO gas mixtures.

CO. Consequently, the C≡O bond gains strength, leading to the observed higher vibrational frequency. In contrast with the CO adsorption experiments, none of the catalysts displayed any bridge-bonded CO bands in these measurements. Hence, we propose that in the presence of hydrogen, the bridge-bonded CO species are very rapidly hydrogenated to hydrocarbons.

The region between 1700 and 1300 cm^{-1} (Fig. 8) reveals the presence of two major bands at around 1590 and 1375 cm^{-1}, which can be assigned to CO_3^{2-} groups bonded to the titania support oxygen atoms [37]. It should be noted that CH_3 and CH_2 bending vibrations also absorb in this region (i.e., around 1450 and 1380 cm^{-1}). However, regarding the absence of a significant band at 1450 cm^{-1}, the peak at around 1375 cm^{-1} is assigned to the O–C–O stretching vibration of surface-bonded monodentate CO_3^{2-} species. The peak at 1570 cm^{-1} and the shoulder at 1330 cm^{-1} are attributed to bidentate-bonded carbonate species. As noted earlier, by increasing the manganese content in the catalysts, the total absorption of the carbonate peaks increases. In this case, differences in peak intensities are relatively large, and for that reason, a semiquantitative analysis was considered. The total intensity of the carbonate absorption bands increases from HCo to $HCo_{20}Mn_5$ almost proportionally to the increase in MnO loading. This indicates that the formation of carbonate species is promoted by the presence of manganese. Because the formation of surface carbonates requires the presence of CO_2, this result suggests that manganese may play a role in catalyzing the conversion of CO to CO_2. Unfortunately, because of the low conversions, no additional proof to verify the increasing water–gas shift activity of the manganese-loaded catalysts could be established from the catalytic tests. However, manganese oxide has been reported to catalyze the water–gas shift reaction [38,39]. This reaction has important implications for FT, significantly affecting product selectivity.

Table 2
FT catalytic performances after 40 h reaction at 1 bar and 220 °C

Sample	Activity[a]	CH_4 (wt%)	C_{5+} (wt%)	Chain growth probability (α)
HCo	0.53	28.4	36.6	0.62
$HCo_{20}Mn_2$	0.72	21.2	43.8	0.64
$HCo_{20}Mn_3$	0.93	20.2	45.1	0.65
$HCo_{20}Mn_4$	0.86	17.3	53.9	0.71
$HCo_{20}Mn_5$	0.87	14.1	61.3	0.77

[a] 10^{-5} mol CO $g\,Co^{-1}\,s^{-1}$.

3.3. Catalysis

The catalytic results obtained after 40 h of reaction are given in Table 2. The presence of manganese clearly affects the selectivity of the catalysts and, to a lesser extent, their activity. The C_{5+} selectivity gradually increases from 36.6 to 61.3 wt% from the unpromoted catalysts to the sample with the highest MnO loading. This increase in C_{5+} selectivity occurs mainly at the expense of CH_4 formation, which is decreased from 28.4 to 14.1 wt% for the HCo and $HCo_{20}Mn_5$ catalysts, respectively. The gradual shift in selectivity displayed by the catalysts loaded with various amounts of MnO is illustrated in Fig. 9.

The product distribution obtained for the different catalysts is in accordance with the Anderson–Schultz–Flory (ASF) kinetics [40]. Using the ASF distribution, we determined the chain growth probability (α) from the slope of the linear part of the plot. The α values change significantly on MnO addition, increasing from $\alpha = 0.62$ for the unpromoted catalyst to $\alpha = 0.77$ for $HCo_{20}Mn_5$. However, the activity reaches a maximum of 0.93×10^{-5} mol CO $g\,Co^{-1}\,s^{-1}$ for MnO loadings of 2.15 wt% and subsequently decreases for higher MnO loadings. These results indicate that loading the catalysts with small amounts of MnO causes the cobalt particles to become more selective to longer hydrocarbon chains. In addition, the activity of the cobalt particles is also increased. Excessive coverage by MnO, however, results in a lowering of the activity, probably because some of the active sites become blocked. The latter was confirmed by the H_2 chemisorption and CO adsorption DRIFTS experiments discussed earlier.

The activity of the different catalysts correlates directly with H_2 uptake in the chemisorption experiments. The highest H_2 uptake is seen in the sample with a MnO loading of 2.15 wt%.

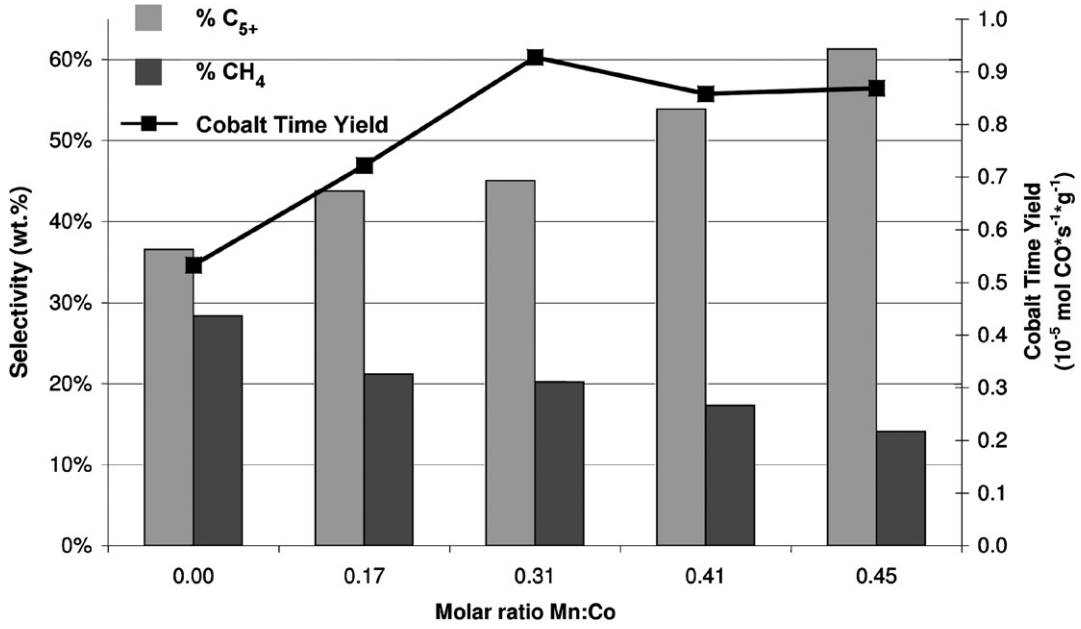

Fig. 9. Influence of the MnO loading on the FT activity and the C_{5+} and CH_4 selectivity of the Co/TiO_2 and $Co/Mn/TiO_2$ catalysts under study.

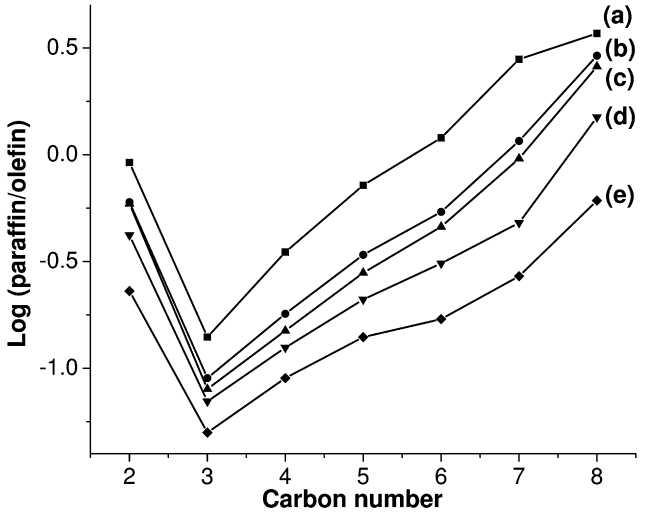

Fig. 10. Influence of MnO on the paraffin to olefin ratio for the HCo (a), $HCo_{20}Mn_2$ (b), $HCo_{20}Mn_3$ (c), $HCo_{20}Mn_4$ (d), and $HCo_{20}Mn_5$ (e) catalysts.

This sample also exhibits the highest activity in the FT reaction. This further confirms the possibly important role of manganese in optimizing the amount of accessible cobalt metal sites by decreasing the interaction between the cobalt phase and the TiO_2 support.

Catalytic testing further showed that the presence of MnO had a profound effect on the paraffin/olefin selectivity of the catalysts. Increasing the MnO loading gradually increased the fraction of olefin products. This effect is illustrated in Fig. 10, which shows the paraffin-to-olefin (P/O) ratio as a function of MnO loading. As shown, the P/O ratios for all of the hydrocarbon fractions are clearly decreasing with increasing MnO loading. This indicates a decreased hydrogenation ability of cobalt particles with the addition of MnO. This effect is directly involved in the increased production of olefins in the Mn-promoted catalysts, because the chain growth termination step by H_2 addition is suppressed. Consequently, the hydrocarbon chains adsorbed at the cobalt surface have a greater chance to grow, thereby resulting in longer hydrocarbon chains as products. We note that strictly paraffin-to-olefin ratios should be compared at the same conversion. However, because lower P/O ratios were observed at higher conversion, the effect of the MnO promoter should be even more pronounced when compared at equal conversion rates.

By comparing the paraffin-to-olefin ratios obtained for the various samples with the linear-to-bridge CO-intensity ratio measured by DRIFTS, it is noteworthy that the appearance of a more intense bridge CO absorption band may suggest that the catalysts are active in hydrogenation reactions, because a bridge-adsorbed CO molecule has a weaker C–O bond and thus can be more easily hydrogenated. The HCo catalyst presented the strongest bridge CO adsorption and also the highest CH_4 selectivity. Hence, a higher relative concentration of bridge-bonded CO species may possibly lead to a low C_{5+} selectivity, because these species are rapidly hydrogenated at the catalyst surface, leading to the formation of mainly CH_4. The results clearly indicate that MnO at the surface of the Co^0 particles suppresses CH_4 formation by decreasing the likelihood of hydrogenation reactions in FT synthesis.

4. Conclusion

The presence of manganese in Co/TiO_2 catalysts results in decreased cobalt reducibility as a result of the intimate association between cobalt and manganese oxide species. At high manganese loading (>2.15 wt%), hydrogen chemisorption is strongly suppressed in $Co/Mn/TiO_2$ catalytic systems as a result of the coverage of cobalt active sites by TiO_x and MnO species. In this respect, the presence of small amounts of manganese appears to increase the available Co^0 surface, presumably by

preventing SMSI between cobalt and TiO_2. Accordingly, catalytic activity reaches a maximum at intermediate manganese loadings.

Except for these *structural* promotion effects, the use of DRIFTS in combination with CO and CO/H_2 demonstrated that MnO remains closely associated with cobalt particles during the FT reaction, acting as an *electronic* promoter on the Co^0 surface sites. Mn^{2+} withdraws electron density from the Co^0 sites, producing a relatively greater amount of linearly bonded CO. This results in a lower hydrogenation rate under FT reaction conditions, as illustrated by the formation of more olefins. As a result, the catalysts have a higher C_{5+} product selectivity.

Finally, adding manganese to the Co/TiO_2 system resulted in an increase in surface carbonate species during the FT reaction. It is suggested that MnO itself is a catalyst for the water–gas shift reaction, converting CO to CO_2 and thereby affecting catalyst performance.

Acknowledgments

The authors gratefully acknowledge Shell Global Solutions for financial support. The authors thank H. Oosterbeek, H. Kuijpers, and C. Mesters (Shell Global Solutions) for their input and fruitful discussions and Fouad Soulimani for his help and support during the DRIFTS experiments.

References

[1] S.E. Colley, R.G. Copperthwaite, G.J. Hutchings, S.P. Terblanche, M.M. Thackeray, Nature 339 (1989) 129.
[2] M.E. Dry, Catal. Today 71 (2002) 227.
[3] H. Schulz, Appl. Catal. A 186 (1999) 3.
[4] F. Morales, B.M. Weckhuysen, Catalysis (Specialist Periodicals Reports, The Royal Society of Chemistry) 19 (2006) 1.
[5] F. Morales, F.M.F. de Groot, O.L.J. Gijzeman, A. Mens, O. Stephan, B.M. Weckhuysen, J. Catal. 230 (2005) 301.
[6] F. Morales, D. Grandjean, F.M.F. de Groot, O. Stephan, B.M. Weckhuysen, Phys. Chem. Chem. Phys. 7 (2005) 568.
[7] F. Morales, D. Grandjean, A. Mens, F.M.F. de Groot, B.M. Weckhuysen, J. Phys. Chem. B 110 (2006) 8626.
[8] F. Morales, F.M.F. de Groot, P. Glatzel, E. Kleimenov, H. Bluhm, M. Havecker, A. Knop-Gericke, B.M. Weckhuysen, J. Phys. Chem. B 108 (2004) 16201.
[9] S.T. Hussain, Ads. Sci. Technol. 13 (1996) 489.
[10] M. Jiang, M. Koizumi, T. Ozaki, M. Yamada, Appl. Catal. A 209 (2001) 59.
[11] K.J. Klabunde, Y. Imizu, J. Am. Chem. Soc. 106 (1984) 2721.
[12] J.L. Zhang, J. Ren, J.G. Chen, Y.H. Sun, Acta Phys. Chim. Sin. 18 (2002) 260.
[13] J.A. Anderson, M.F. Garcia (Eds.), Supported Metals in Catalysis, Imperial College Press, London, 2005.
[14] A. Davydov, Molecular Spectroscopy of Oxide Catalyst Surfaces, Wiley, New York, 2003.
[15] Y. Marcus, Ion Properties, Dekker, New York, 1997.
[16] J.W. Niemantsverdriet, Spectroscopy in Catalysis, VCH Verlag, Weinheim, 1993.
[17] T. Visser, T.A. Nijhuis, A.M.J. van der Eerden, K. Jenken, Y. Ji, W. Bras, S. Nikitenko, Y. Ikeda, M. Lepage, B.M. Weckhuysen, J. Phys. Chem. B 109 (2005) 3822.
[18] B.M. Weckhuysen (Ed.), In Situ Spectroscopy of Catalysts, American Scientific Publishers, Stevenson Ranch, 2004.
[19] A.A. Davydov, M.P. Komarova, V.F. Anufrienko, N.G. Maksimov, Kinet. Katal. 14 (1973) 15.
[20] V.B. Kazansky, A.V. Zaitsev, V.Y. Borovkov, A.L. Lapidus, Appl. Catal. 40 (1988) 17.
[21] B. Mothebe, D.J. Duvenhage, V.D. Sokolovskii, Stud. Surf. Sci. Catal. 107 (1997) 1.
[22] J. Ryczkowski, Catal. Today 68 (2001) 263.
[23] R.A. van Santen, P.W.N.M. van Leeuwen, J.A. Moulijn, B.A. Averill (Eds.), Catalysis: An Integrated Approach, second, revised and enlarged ed., Elsevier, Amsterdam, 1999, p. 508.
[24] B.L. Mojet, J.T. Miller, D.C. Koningsberger, J. Phys. Chem. B 103 (1999) 2724.
[25] A.J. van Dillen, J.W. Geus, L.A.M. Hermans, J. van der Meijden, Stud. Surf. Sci. Catal. 2 (1997) 677.
[26] R.C. Reuel, C.H. Bartholomew, J. Catal. 85 (1984) 63.
[27] Q. Liang, K. Chen, W. Hou, Q. Yan, Appl. Catal. A 166 (1998) 191.
[28] J.L. Martin de Vidales, E. Vila, R. Rojas, O. Garcia, Chem. Mater. 7 (1995) 1716.
[29] G.L. Haller, D.E. Resasco, Adv. Catal. 36 (1989) 173.
[30] M.A. Vannice, J. Catal. 11 (1982) 225.
[31] T. Komaya, A.T. Bell, Z. Wengsieh, R. Gronsky, F. Engelke, T.S. King, M. Pruski, J. Catal. 149 (1994) 142.
[32] G.L. Bezemer, P.B. Radstake, U. Falke, H. Oosterbeek, A.J. van Dillen, K.P. de Jong, J. Catal. 237 (2006) 152.
[33] G.L. Bezemer, P.B. Radstake, V. Koot, A.J. van Dillen, J.W. Geus, K.P. de Jong, J. Catal. 237 (2006) 291.
[34] G.L. Bezemer, U. Falke, A.J. van Dillen, K.P. de Jong, Chem. Commun. 6 (2005) 731.
[35] A.A. Davydov, N. Coville, Russ. Chem. Bull. 44 (1995) 1866.
[36] K. Nakamoto, Infrared and Raman Spectra of Inorganic and Coordination Compounds, Part B, Applications in Coordination, Organometallic, and Bioinorganic Chemistry, fifth ed., Wiley, New York, 1997.
[37] L.F. Liao, C.F. Lien, D.L. Shieh, M.T. Chen, J.L. Lin, J. Phys. Chem. B 106 (2002) 43.
[38] M.J. Keyser, R.C. Everson, R.L. Espinoza, Appl. Catal. A 171 (1998) 99.
[39] T. Riedel, M. Claeys, H. Schulz, G. Schaub, S.S. Nam, K.W. Jun, M.J. Choi, G. Kishan, K.W. Lee, Appl. Catal. A 186 (1999) 201.
[40] E. Iglesia, Appl. Catal. A 161 (1997) 50.